JOURNAL OF GEOPHYSICAL RESEARCH, VOL. 111, D15209, doi:10.1029/2005JD006784, 2006

New dual-frequency microwave technique for retrieving liquid water path over land

M. N. Deeter[1] and J. Vivekanandan[1]

Received 19 October 2005; revised 7 March 2006; accepted 9 May 2006; published 8 August 2006.

[1] We present and demonstrate a new methodology for retrieving liquid water path over land using satellite-based microwave observations. As input, the technique exploits Advanced Microwave Scanning Radiometer for EOS (AMSR-E) brightness temperature polarization-difference signals at 37 and 89 GHz. Regression analysis performed on model simulations indicates that over variable atmospheric and surface conditions these polarization-difference signals can be simply parameterized in terms of the surface emissivity polarization-difference ($\Delta\epsilon$), surface temperature, liquid water path (LWP), and precipitable water vapor (PWV). By exploiting the weak frequency dependence of $\Delta\epsilon$, a simple expression is obtained which enables fast and direct (noniterative) retrievals of LWP. The new methodology is demonstrated and validated using several months of AMSR-E observations over (1) the Southern Great Plains (SGP) of the United States and (2) an area near Montreal, Canada, instrumented during the Alliance Icing Research Study II (AIRS II) field campaign. Comparisons are also made with MODIS LWP retrieval results for one scene over the SGP region. Retrieval results in clear-sky conditions indicate an uncertainty on the order of 0.06 mm, in agreement with theoretical estimates. In cloudy conditions, results using the new method are systematically smaller than results for both ground-based microwave radiometers and MODIS but are well correlated.

Citation: Deeter, M. N., and J. Vivekanandan (2006), New dual-frequency microwave technique for retrieving liquid water path over land, *J. Geophys. Res.*, *111*, D15209, doi:10.1029/2005JD006784.

1. Introduction

[2] Measurements of cloud liquid water properties are important in a wide range of disciplines including climate change [*Slingo*, 1989], numerical weather prediction (NWP) [*Ohring et al.*, 2002] and aircraft icing [*Riley*, 1998]. A variety of remote sensing techniques have been developed to address this need, including both visible/infrared [*Dong et al.*, 2002] and microwave methods. Unlike visible and infrared radiation, microwaves with frequencies of 90 GHz and less are insensitive to nonprecipitating cloud ice particles [*Muller et al.*, 1994], and are unaffected by the liquid cloud particle size distribution. Both of these features are desirable for characterizing cloud properties such as liquid water content (LWC) and liquid water path (LWP). Passive microwave techniques are particularly mature for (1) ground-based LWP retrievals [*Liljegren et al.*, 2001a] and (2) satellite-based LWP retrievals over the oceans [*Weng and Grody*, 1994]. Satellite-based methods for retrieving LWP over land are less mature [*Aires et al.*, 2001; *Greenwald et al.*, 1997]. The main issue inhibiting satellite-based microwave retrievals of LWP over land so far has been discriminating cloud features from surface effects.

[3] Because of the high atmospheric transmittance of microwaves (even in the presence of clouds), land-surface temperature and emissivity variations directly modulate observed satellite microwave brightness temperatures. Moreover, the relatively high mean surface emissivity values typical of land surfaces (compared to ocean surfaces) result in poor thermal contrast conditions. Thus, at microwave frequencies, the same liquid cloud would produce a much larger radiative perturbation (in terms of the observed brightness temperature, T_B) over the ocean than over land. The "Normalized Polarization Difference" (NPD) retrieval technique was developed specifically to overcome these limitations [*Greenwald et al.*, 1997, 1999a; *Combs et al.*, 1998]. This technique exploits the Special Sensor Microwave/Imager (SSM/I) 85 or 37 GHz polarization-difference signals ($\Delta T_B = T_B^V - T_B^H$). The technique relies on (1) the small (but finite) difference in land-surface emissivity associated with the V and H polarization states and (2) the depolarizing effect of absorption of microwaves by liquid clouds. Compared to techniques based on a single SSM/I signal, the NPD technique was shown to be much less sensitive to cloud height, surface temperature and systematic instrumental errors. Drawbacks of the NPD technique (as presented by Greenwald et al.) included the need for synchronized radiosonde measurements and visible/infrared satellite observations as ancillary input data, the need for prior knowledge of the surface emissivity polarization difference ($\Delta\epsilon = \epsilon^V - \epsilon^H$), and a computationally expensive iterative retrieval algorithm. These issues have

[1]Research Applications Laboratory, National Center for Atmospheric Research, Boulder, Colorado, USA.

0148-0227/06/2005JD006784$09.00

so far prevented the development of an operational satellite product.

[4] In the following, we describe a new regression-based technique for retrieving LWP in nonprecipitating clouds over land. The technique is applied specifically to the Advanced Microwave Scanning Radiometer for EOS (AMSR-E) instrument, but could be easily adapted to exploit SSM/I observations. The retrieval methodology exploits polarization-difference signals, like the NPD technique, but incorporates additional features which circumvent the main problems of the NPD technique listed above. Specifically, the new method involves no coordinated measurements from any other instruments (either ground-based or satellite-based), does not depend on prior knowledge of $\Delta\epsilon$, and is based on a simple analytical expression.

[5] The remainder of the paper is organized as follows. In section 2, model simulations are presented which lead to the development of a simple parameterization relating the observed polarization-difference signals (ΔT_B) to two surface parameters ($\Delta\epsilon$ and T_S) and two atmospheric parameters (LWP and precipitable water vapor, PWV). In section 3, the methodology for retrieving LWP using the parameterization developed in section 2 is outlined, along with an analysis of potential errors. Preliminary validation results are presented in section 4 and analyzed in section 5. Validation is based on observations (1) over the ARM (Atmospheric Radiation Measurements) SGP (Southern Great Plains) study area in Oklahoma during a three month period spanning 2003 and 2004 and (2) over an area including the Mirabel airport near Montreal, Canada. AMSR-E results are also compared to retrievals based on the MODIS (Moderate resolution Imaging Spectrometer) satellite instrument for one overpass of the SGP region. Conclusions are offered in section 6.

2. Radiative Transfer Modeling

[6] The radiative transfer model used to calculate AMSR-E brightness temperatures was adapted directly from a plane-parallel model described previously [*Deeter and Vivekanandan*, 2005]. Atmospheric profiles of temperature, water vapor, and LWC (i.e., liquid mass per unit volume) and surface parameters (temperature and emissivity) are required model inputs. For specified atmospheric states, layer absorption optical depths were calculated over the spectral ranges corresponding to the AMSR-E 37 and 89 GHz channels using the MONORTM radiative transfer code from Atmospheric and Environmental Research, Inc. (available at http://rtweb.aer.com). Layer optical depths were calculated on a grid with 0.5 km vertical resolution and at spectral resolutions of 0.010 and 0.020 cm^{-1} for the 37 and 89 GHz channels, respectively. Absorption due to both gases and cloud liquid water particles is explicitly included in the layer optical depth calculations. The effects of scattering from nonprecipitating liquid and ice cloud particles at the AMSR-E frequencies are generally very weak [*Muller et al.*, 1994] and are neglected in the model. Under this approximation, the radiative properties of the liquid cloud particles depend on the LWC, but not on the liquid particle size distribution. Precipitating clouds are radiatively much more complex than nonprecipitating clouds, and are not considered in this paper.

2.1. Model Inputs

[7] Development of a regression-based retrieval method for LWP requires a "training set" of atmospheric profiles which adequately represent variability in all parameters relevant to the calculation of microwave brightness temperatures: temperature, water vapor, and LWC. Four training sets were produced for this study using two alternative methods. The ultimate influence of the training set on the retrieval results is explored in section 5. The first method exploits retrieved profiles of temperature, water vapor and LWC produced using the ground-based twelve-channel Microwave Radiometer Profiler (MWRP) [*Liljegren et al.*, 2001b; *Gueldner and Spaenkuch*, 2001]. All MWRP profiles acquired at the ARM SGP Central Facility during December 2001 were used to form the training set "M1." MWRP profiles were typically generated every 30 minutes. The estimated accuracy of MWRP temperature and water vapor retrievals are 2 K and 2 gm^{-3}, respectively [*Liljegren et al.*, 2001b].

[8] The second method relies on analyzed profiles of temperature and water vapor from the National Center for Environmental Prediction (NCEP). Unlike the MWRP training set profiles, analyzed meteorological data enable the simulation of microwave brightness temperatures for regions distinctly different than the ARM SGP site. The main obstacle to the use of these profiles for producing a training set is the lack of analyzed LWC profiles. Following similar methods [*Liljegren et al.*, 2001a], we constructed synthesized LWC profiles based on the NCEP relative humidity and temperature profiles. For each profile, LWC is set to a random value (between 0.0 and 0.5 gm^{-3}) in each 0.5-km-thick layer for which both the mean RH and temperature are found to be above threshold values (typically 90% and 253 K). NCEP-based training sets were produced to represent three temporal/spatial domains. For direct comparisons against the MWRP training set, the "N1" set was produced only on the basis of NCEP reanalysis for the ARM SGP region for December 2001. Individual profiles were produced for each 6-hour interval represented in the NCEP product. NCEP-based profile sets were also generated for the SGP region for all of 2001 ("N2"), and for a much larger North American midlatitude region (bounded by 30N, 60N, 130W and 60W) for all of 2001 ("N3"). The latter two training sets were used to evaluate possible retrieval biases due to the use of regression coefficients based on increasingly general seasonal and geographical regimes. Results of those tests are described in section 4.

2.2. Regression Analysis

[9] The radiative transfer equation describing the relationship between ΔT_B, $\Delta\epsilon$, the surface temperature T_S, the atmospheric temperature profile, and the atmospheric transmittance profile was originally derived in [*Greenwald et al.*, 1997]. The equation was presented later in simplified form in the work by *Combs et al.* [1998] as

$$\Delta T_B = \Delta\epsilon(T_S - T_D)\mathcal{T} \tag{1}$$

where T_D is the brightness temperature corresponding to the downwelling radiation at the surface (from atmospheric emission) and $\mathcal{T}$ is the total atmospheric transmittance

Table 1. Regression Coefficients (as Determined by Applying Multiple Linear Regression to Equation (3)) and Parameterization Error σ for PDP Training Sets Described in Section 2.1[a]

PDP Training Set	Channel	β_0	β_1, K^{-1}	β_2, m^2/kg	β_3, m^2/kg	σ
M1	37 GHz	4.28	0.00435	−0.839	−0.00597	0.0077
M1	89 GHz	3.91	0.00539	−3.34	−0.0299	0.0137
N1	37 GHz	4.13	0.00489	−0.849	−0.00568	0.0136
N1	89 GHz	3.24	0.00791	−3.38	−0.0302	0.0260
N2	37 GHz	4.16	0.00481	−0.852	−0.00641	0.0144
N2	89 GHz	2.92	0.00916	−3.31	−0.0318	0.0407
N3	37 GHz	4.05	0.00507	−0.920	−0.00652	0.0274
N3	89 GHz	3.29	0.00751	−3.28	−0.0325	0.0571

[a]Values of β and σ assume that ΔT_B values are expressed in K.

(from the surface to TOA). Equation (1) is exactly valid at a single microwave frequency only; comparisons with actual ΔT_B measurements formally require spectral integration of equation (1) over the instrumental bandpass. Atmospheric parameters including the temperature, water vapor and LWC profiles are needed to evaluate both T_D and $\mathcal{T}$. In the original NPD technique, iterative retrievals of LWP were based on equation (1), where the atmospheric terms T_D and $\mathcal{T}$ were recalculated for each iteration. Values of $\Delta\epsilon$ were retrieved from prior clear-sky SSM/I observations, and temperature and water vapor profiles required to calculate T_D and $\mathcal{T}$ were obtained from nearby radiosonde measurements. For operational LWP retrievals, we seek an approximation to equation (1) which (1) requires no numerical integration and (2) allows direct (noniterative) calculation of LWP in terms of ΔT_B.

2.2.1. Linearization

[10] We have determined that the RHS of equation (1) may be accurately approximated in terms of two surface parameters ($\Delta\epsilon$ and T_S) and two column-integrated atmospheric parameters (LWP and PWV). Justifications for this approximation are based on theoretical grounds and empirical observations. First, in the limit of an isothermal atmosphere, the dependence of ΔT_B on atmospheric terms is dominated by the dependence on the atmospheric transmittance $\mathcal{T}$. This point is demonstrated in Appendix A. At the microwave frequencies considered in this paper, $\mathcal{T}$ varies primarily with respect to path-integrated absorber amounts (i.e., LWP and PWV); the vertical distribution of liquid water and water vapor is relatively unimportant. Moreover, as demonstrated below, regression-based fits of ΔT_B to these four parameters yield negligibly small residual errors.

[11] Regression-based coefficients are needed to independently describe the dependence of ΔT_B on T_S, LWP, and PWV. The exact proportionality of ΔT_B and $\Delta\epsilon$ (as indicated by equation (1)) implies that no coefficient is needed for $\Delta\epsilon$. Furthermore, the exponential dependence of $\mathcal{T}$ on both LWP and PWV (as in Beer's Law) suggests that equation (1) should be parameterized in the form

$$\Delta T_B \approx \Delta\epsilon \exp(\beta_0 + \beta_1 T_S + \beta_2 LWP + \beta_3 PWV) \qquad (2)$$

where the β_i values are fitting coefficients to be determined. Hereafter we refer to equation (2) as the "Polarization-Difference Parameterization," or PDP. The inclusion of the coefficient β_0 is necessary to account for (1) absorption by fixed gases (mainly O_2) and (2) the zeroth-order approximation to the term ($T_S - T_D$) in equation (1). After dividing both sides by $\Delta\epsilon$ and applying the natural logarithm, we find that

$$\ln\left(\frac{\Delta T_B}{\Delta\epsilon}\right) \approx \beta_0 + \beta_1 T_S + \beta_2 LWP + \beta_3 PWV \qquad (3)$$

For retrievals of LWP, equation (3) is significant because (1) it linearly relates a measurable quantity to the desired retrieval parameter (in a way that permits the use of multiple linear regression) and (2) it directly facilitates the use of observations at two frequencies (as described further in section 3).

2.2.2. Regression Results

[12] Values of the PDP regression coefficients β_i were determined for the AMSR-E 37 and 89 GHz channels using the various training sets described in section 2.1, and are listed in Table 1. The fit of the regression for training set M1 is shown graphically in Figure 1. The use of logarithmic scaling on the vertical axes clearly exposes the exponential dependence of ($\Delta T_B/\Delta\epsilon$) on the quantity ($\beta_0 + \beta_1 T_S + \beta_2 LWP$

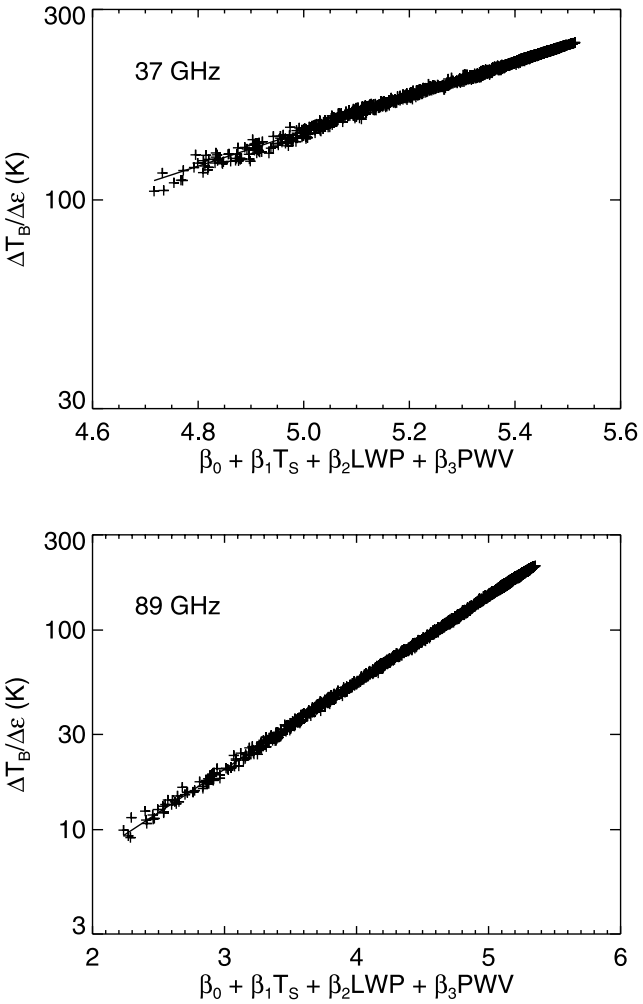

Figure 1. Results of multiple linear regression applied to equation (3) for both the 37 and 89 GHz AMSR-E polarization-difference signals. Plotted points indicate results of radiative transfer simulations described in section 2, applied to training set "M1." Solid line indicates best fit as determined by regression analysis.

+ $\beta_3 PWV$). Plotted data points in each panel correspond to the individual training set profiles (and model-calculated brightness temperatures) which are the basis of the regression. Solid lines indicate the best fit result from multiple linear regression. Figure 1 demonstrates that the PDP provides an accurate approximation to equation (1) over widely varying atmospheric conditions. As indicated in Table 1, regression coefficients for training sets N1, N2, and N3 are quantitatively similar (to within about 20%) to those for M1.

3. Regression-Based Retrieval Algorithm

3.1. Variability of $\Delta\epsilon$

[13] Even if exact values for T_S and PWV were independently available, single-frequency retrievals of LWP based on equation (3) would be severely inhibited by the variability of $\Delta\epsilon$. Within the NPD technique, $\Delta\epsilon$ is retrieved independently using prior clear-sky observations (as determined using coincident infrared measurements) and is assumed to be stable over the period between the clear-sky and cloudy overpasses. At SSM/I frequencies, $\Delta\epsilon$ varies over land from approximately 0.06 to near zero [*Prigent et al.*, 1997; *Lin and Minnis*, 2000; *Ruston and Vonder Haar*, 2004]. Variability of $\Delta\epsilon$ is associated with properties of vegetation, surface roughness, soil moisture, and snow cover. However, coincident retrievals of land surface emissivity at 37 and 85 GHz (based on SSM/I observations) demonstrate that $\Delta\epsilon$ is only weakly frequency-dependent [*Prigent et al.*, 1997; *Lin and Minnis*, 2000; *Ruston and Vonder Haar*, 2004]. For example, over the United States, reported summertime $\Delta\epsilon$ values for the SSM/I 37 and 85 GHz channels differ by less than 20% for each of four vegetation classes (bare, grass, crop, and forest) [*Ruston and Vonder Haar*, 2004]. Thus, to a first approximation, the frequency dependence of $\Delta\epsilon$ may be neglected (at least with respect to the 37 and 85 GHz channels).

3.2. Dual-Frequency Methodology

[14] In applications where $\Delta\epsilon$, T_S and PWV are known a priori, equation (3) could be directly inverted to retrieve LWP using a single polarization-difference signal, i.e.,

$$LWP = \frac{\ln\left(\frac{\Delta T_B}{\Delta\epsilon}\right) - \beta_0 - \beta_1 T_S - \beta_3 PWV}{\beta_2} \tag{4}$$

[15] Development of an LWP retrieval equation based on polarization-difference signals for two frequencies (specifically, 37 and 89 GHz) is also straightforward. Dividing the expression (based on equation (3)) for $\Delta T_B^{89}/\Delta\epsilon^{89}$ by the expression for $\Delta T_B^{37}/\Delta\epsilon^{37}$ and solving for LWP yields

$$LWP = \frac{\ln\left(\frac{\Delta T_B^{89}}{\Delta T_B^{37}}\right) - \ln\left(\frac{\Delta\epsilon^{89}}{\Delta\epsilon^{37}}\right) - \left(\beta_0^{89} - \beta_0^{37}\right) - \left(\beta_1^{89} - \beta_1^{37}\right) T_S - \left(\beta_3^{89} - \beta_3^{37}\right) PWV}{\beta_2^{89} - \beta_2^{37}} \tag{5}$$

[16] Therefore, if the frequency dependence of $\Delta\epsilon$ is negligible (or, specifically, if $\Delta\epsilon^{89}/\Delta\epsilon^{37}$ can be shown to vary negligibly), LWP may be retrieved without any a priori knowledge of $\Delta\epsilon$. In practical terms, the dual-frequency methodology is an improvement over the single-frequency method because (1) it requires no independent clear/cloudy determination (which would involve measurements from a separate instrument) and (2) it involves no assumptions regarding the temporal variability of $\Delta\epsilon$. Moreover, as a "stand-alone" retrieval algorithm, the dual-frequency methodology is more generally applicable than the NPD method (which requires independent visible/infrared satellite observations to determine scene cloudiness). For example, the presence of overlying cirrus clouds does not directly inhibit LWP retrievals using the dual-frequency method. Also, the dual-frequency method is applicable to regions of persistent cloudiness, which would be problematic for the single-frequency method.

3.2.1. Data Gridding

[17] Uncertainties for LWP retrievals based on the NPD technique (using the SSM/I 85 GHz channel) were found to be dominated by instrumental noise and the uncertainty in $\Delta\epsilon$ [*Greenwald et al.*, 1999a]. The sensitivity (defined as the noise-equivalent T_B) of the SSM/I 85 GHz channel is 0.7 K [*Hollinger et al.*, 1990], whereas the reported sensitivity of the AMSR-E 89 GHz channel is 1.1 K [*Njoku et al.*, 2003]. Considered by itself, the higher noise figure for AMSR-E indicates that application of the NPD technique directly to AMSR-E observations should result in relatively larger retrieval errors. However, compared to the SSM/I instrument, the instantaneous field of view (or "footprint") of the AMSR-E observations is substantially smaller and the sampling density (i.e., number of observations per unit area) substantially higher. For example, the SSM/I 85 GHz channel footprint measures approximately 15 by 13 km, whereas the footprint for the AMSR-E 89 GHz channel measures approximately 6 by 4 km.

[18] Using data averaging, the greater sampling density of AMSR-E observations may be used to offset the slightly greater instrumental noise. The dual-frequency technique demonstrated in section 4 incorporates data averaging within a simple gridding algorithm. A rectangular 0.25° by 0.25° latitude/longitude grid was employed for the current study. In midlatitude regions, each grid cell typically captures between 25 and 30 AMSR-E 89 GHz observations in each overpass. Assuming a square root reduction in the effective instrumental noise with number of observations (applicable to random Gaussian noise processes), the estimated effective grid cell-scale instrumental noise for 89 GHz observations is reduced from 1.1 K to approximately 0.2 K. For 37 GHz observations, the sampling density is four times smaller than for 89 GHz, whereas the instrumental noise is about a factor of two smaller [*Njoku et al.*, 2003]. Thus the grid cell scale instrumental noise for 37 GHz observations is also approximately 0.2 K.

3.2.2. Error Analysis

[19] We consider retrieval errors due to the following effects. First, parameterization errors for both the 37 and 89 GHz channels (as quantified by σ in Table 1) are directly

Table 2. Parameter Values Used to Calculate σ_{LWP} (Equation (6)) as a Function of LWP (See Section 3.2.2)

Parameter	Value
σ_{89}	0.3 K
σ_{37}	0.3 K
$R(\epsilon)$	1.0
$\sigma_{R(\epsilon)}$	0.1
T_S	278.0 K
σ_{TS}	5.0 K
PWV	20.0 kg/m^2
σ_{PWV}	3.0 kg/m^2

associated with the use of equation (3). Second, the methods used to form the training set profiles affect the regression coefficients and therefore may also contribute to retrieval error. Third, errors in ancillary geophysical data (specifically T_S and PWV) directly propagate into LWP retrieval errors. Fourth, instrumental noise may degrade retrieval performance, even with the use of gridding. Finally, uncertainty in the ratio $\Delta\epsilon^{89}/\Delta\epsilon^{37}$ will also contribute to LWP retrieval errors. Contributions to the error budget from other sources, including scattering from precipitation-sized liquid and ice particles, and subgrid LWP variability will likely depend on meteorological conditions and are more difficult to assess; these will be addressed in future studies. (As discussed in section 3.2.3, observations affected by precipitation are avoided by application of a scattering-based filter.)

[20] Excluding the effect of "training set errors" (which are analyzed further in section 5), we estimate the retrieval uncertainty σ_{LWP} by applying "propagation of errors" analysis to equation (5). The resulting error variance for the dual-frequency LWP product is

$$\sigma_{LWP}^2 = \frac{\frac{\sigma_{89}^2}{\left(\Delta T_B^{89}\right)^2} + \frac{\sigma_{37}^2}{\left(\Delta T_B^{37}\right)^2} + \frac{\sigma_{R(\epsilon)}^2}{R(\epsilon)^2} + \sigma_{TS}^2\left(\beta_1^{89} - \beta_1^{37}\right)^2 + \sigma_{PWV}^2\left(\beta_3^{89} - \beta_3^{37}\right)^2 + \sigma_{P89}^2 + \sigma_{P37}^2}{\left(\beta_2^{89} - \beta_2^{37}\right)^2} \tag{6}$$

where σ_{89} and σ_{37} are the instrumental errors associated with ΔT_B^{89} and ΔT_B^{37}, $\sigma_{R(\epsilon)}$ is the uncertainty of the ratio $R(\epsilon)$ (i.e., $\Delta\epsilon^{89}/\Delta\epsilon^{37}$), σ_{TS} and σ_{PWV} are the uncertainties of T_S and PWV, and σ_{P89} and σ_{P37} are the parameterization errors (i.e., residual errors in the quantity $\ln(\Delta T_B/\Delta\epsilon)$) at 89 and 37 GHz which are listed in Table 1.

[21] Typically, retrieval uncertainty is dominated by the terms containing $\sigma_{R(\epsilon)}$, σ_{PWV} and σ_{89}. Together these terms contribute nearly 90% of the total variance. Terms associated with σ_{TS} and parameterization errors are relatively small. The dependence of σ_{LWP} on both $\Delta\epsilon$ and LWP was calculated using equation (6) with the parameter values listed in Table 2. Values for σ_{89} and σ_{37} assume uncorrelated errors in grid cell mean values of T_B^V and T_B^H of 0.2 K (at both 37 and 89 GHz). Values of ΔT_B^{37} and ΔT_B^{89} needed to calculate σ_{LWP} were obtained using equation (2); both LWP and $\Delta\epsilon$ were treated as independent variables. Assumed values for $R(\epsilon)$ and $\sigma_{R(\epsilon)}$ of 1.0 and 0.1 are consistent with reported $\Delta\epsilon$ values at 37 and 85 GHz for common classes of vegetated surfaces of the continental United States [*Ruston and Vonder Haar*, 2004]. The results are plotted in Figure 2 for discrete values of $\Delta\epsilon$ ranging from 0.01 to 0.05. The results demonstrate that σ_{LWP} increases monotonically with LWP but decreases with increasing $\Delta\epsilon$. For $\Delta\epsilon$ values less than about 0.01, σ_{LWP} is typically comparable to or greater than the actual LWP; for such surfaces the method proposed here would only have marginal value. However, for $\Delta\epsilon$ values of 0.02 and larger, σ_{LWP} is less than 0.1 mm for LWP values up to 0.3 mm. Reported values of $\Delta\epsilon$ for various surface types in the United States indicate that values of 0.02 and larger are commonplace except in forested regions.

3.2.3. Cloud Temperature Effects

[22] Significantly, the LWP retrieval algorithm described by equation (5) does not require an a priori estimate of cloud height or temperature. However, at microwave frequencies, absorption coefficients for liquid water are known to be temperature-dependent. This dependence must be considered as a source of potential retrieval error in microwave-based LWP retrieval algorithms [*Liljegren et al.*, 2001a; *Zuidema et al.*, 2005]. By the nature of the method used to produce the synthetic LWC profiles (described in section 2.1), the effect of cloud temperature as a source of retrieval error in the method we describe is included in the parameterization errors σ_{89} and σ_{37}. These errors were found to constitute an insignificant component of σ_{LWP}.

[23] Nevertheless, we have modeled the effect of cloud temperature on retrieval error explicitly. For this study, T_B^V and T_B^H values were calculated at 37 and 89 GHz for varying LWP and cloud height and then fed to the LWP retrieval equation. The radiative transfer model used for these calculations employs the standard Liebe model [*Liebe et al.*, 1991] to estimate the dielectric properties of liquid water as a function of temperature and frequency. Cloud thickness was fixed at 1 km. In this simulation, all other sources of retrieval error (e.g., PWV uncertainty) were eliminated by feeding the LWP retrieval equation the exact corresponding value used in the forward model calculations. Results of this study are presented in Figure 3 for base atmospheric profiles representing typical midlatitude summer (MLS) and winter (MLW) conditions [*McClatchey et al.*, 1972]. Cloudtop temperatures varied between 261.0 and 285.0 K for the MLS atmosphere and between 243.7 and 265.2 K for the MLW atmosphere. LWP retrievals were produced using the "N3" regression coefficients. The simulation results demonstrate that LWP retrieval errors due to cloud temperature variability are typically less than 5%. As indicated by Figure 2, overall retrieval errors are typically much larger than 5%.

3.2.4. Data Quality

[24] Observations affected by scattering from either precipitating particles or surface snow cover are not adequately described by equation (5) and may therefore not be retrievable. Fortunately, the application of SSM/I and AMSR/E observations to the identification of both precipitation and snow cover is well developed. For the current study, observations affected by precipitation or snow cover were

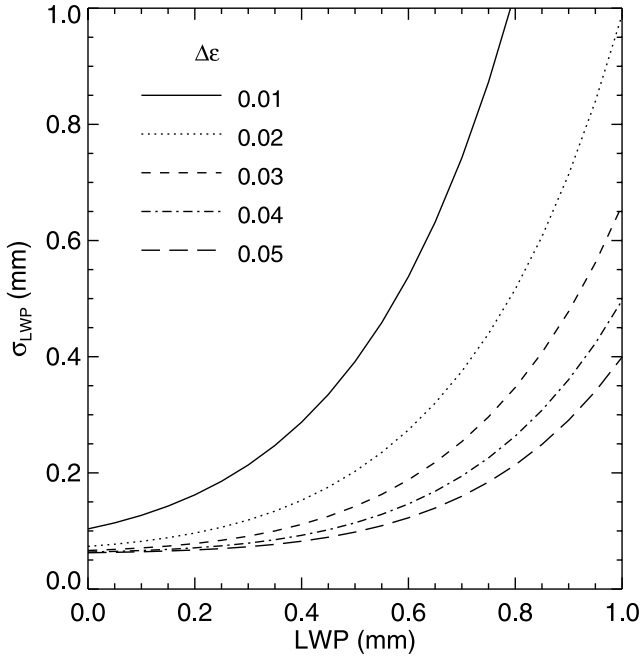

Figure 2. Dependence of LWP retrieval uncertainty on LWP (as calculated according to equation (6)) using parameter values listed in Table 2.

identified using the land-based scattering index described by *Ferraro et al.* [1994].

4. Validation

[25] The dependence of retrieval performance on land surface type (through $R(\epsilon)$) indicates that retrieval errors may exhibit a significant geographic dependence. In this section, we present comparisons of retrieval results based on equation (5) with ground-based LWP measurements for two distinctly different geographic areas in North America. In both cases, the regions were selected primarily because of the availability of ground-based microwave radiometers for providing independent LWP retrieval data (i.e., "ground truth"). The use of two-channel ground-based microwave radiometers operating near 20 and 31 GHz is a common method for validating satellite retrievals of LWP [*Greenwald et al.*, 1999b; *Dong et al.*, 2002]. However, the vast disparity in the sampling area of ground-based radiometers and the satellite-based method being evaluated here poses a significant problem for validation, especially in scenes with large LWP spatial variability [*Wentz and Meissner*, 2000].

4.1. Validation Sites

4.1.1. Southern Great Plains, United States

[26] As part of the Atmospheric Radiation Measurements (ARM) program operated by the United States' Department of Energy, five ground-based microwave radiometers (MWR) distributed throughout the Southern Great Plains (SGP) field site provide near-continuous observations of LWP [*Liljegren et al.*, 2001a]. MWR retrieval data from instruments stationed at the SGP C1 (36.605°N, 97.486°W), B1 (38.305°N, 97.301°W), B4 (36.071°N, 99.218°W), B5 (35.688°N, 95.856°W), and B6 (34.985°N, 97.522°W) facilities were acquired for the period between 1 November 2003 and 31 January 2004 in order to validate AMSR-E retrievals. All AMSR-E observations located within 0.25° by 0.25° latitude/longitude boxes centered on the coordinates of each MWR were extracted, processed with the dual-frequency retrieval methodology and matched with corresponding LWP values from the corresponding MWR. A total of 570 pairs of AMSR-E and MWR retrievals were produced for the three month period. In order to evaluate the role played by the training sets used to produce the PDP regression coefficients, retrievals were performed with all four sets of regression coefficients listed in Table 1.

4.1.2. Montreal, Quebec, Canada

[27] The Alliance Icing Research Study II (AIRS II) was a joint effort by research centers in the United States, Canada, and Europe (see http://airs-icing.org/AIRS_II/AIRS_II.htm) to improve methods for detecting and forecasting aircraft icing conditions. AIRS II was conducted in the vicinity of Montreal, Canada (principally near the Mirabel airport), from November 2003 to March 2004. Retrievals of LWP using a ground-based two-channel microwave radiometer deployed at the Mirabel airport were produced from observations beginning 1 November and ending 14 December. For this period, all AMSR-E observations extracted within the 0.25° by 0.25° latitude/longitude box centered on 45.67°N and 74.03°W were processed using regression set M1 and matched with simultaneous MWR retrievals. A total of 45 matched pairs of AMSR-E and MWR retrievals were produced for the AIRS II period.

4.2. Results

4.2.1. MWR Comparisons

[28] Comparisons of AMSR-E based and MWR-based LWP retrievals for the SGP and AIRS II data sets are

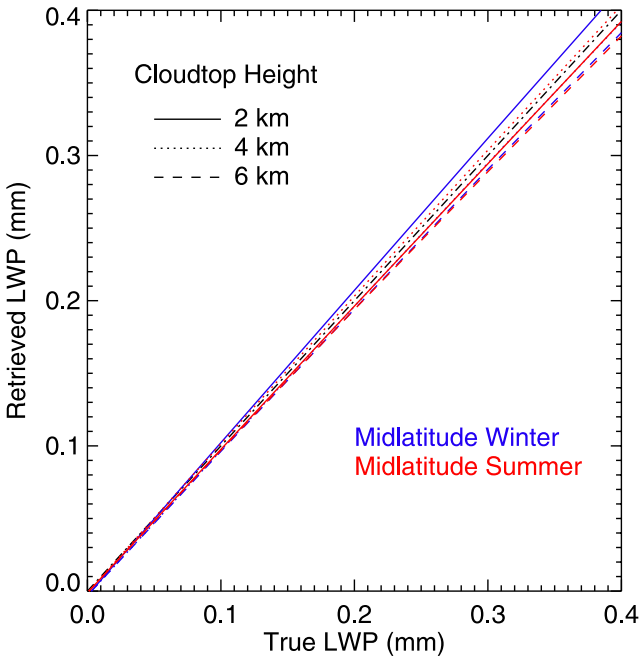

Figure 3. Retrieval simulation results demonstrating effect of cloud height (and implicitly cloud temperature) as source of retrieval error. Over the range of cloud heights from 2 to 6 km, retrieval errors for both midlatitude summer and winter conditions are less than 5%.

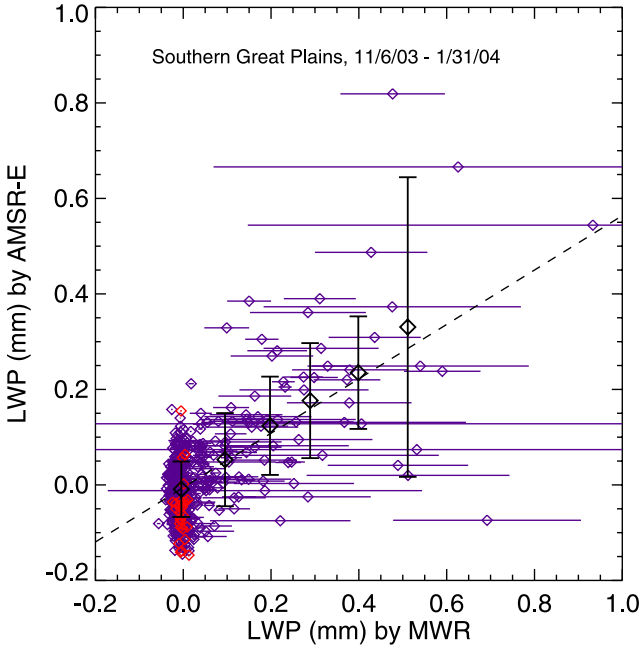

Figure 4. Scatterplot of LWP values retrieved using the AMSR-E dual-frequency method and corresponding MWR values in the Southern Great Plains region between November 2003 and January 2004. AMSR-E retrievals for which brightness temperatures indicated high scattering are plotted in red. Small purple diamonds indicate results for individual overpasses; corresponding horizontal error bars indicate MWR LWP variability over a 2-hour period spanning the time of the AMSR-E overpass. Large black diamonds indicate results binned according to mean MWR value; corresponding vertical error bars indicate the AMSR-E LWP variability within each bin. Parameters for least squares fit line (dashed) are listed in Table 3.

presented as scatterplots in Figures 4 and 5 and are summarized statistically in Table 3. Each point in Figures 4 and 5 corresponds to a single AMSR-E overpass matched with a single MWR. AMSR-E retrieval results shown in Figures 4 and 5 are based on the M1 regression coefficients. In Figures 4 and 5, retrievals for which AMSR-E brightness temperatures indicate scattering (according to the Ferraro algorithm) are plotted in red; approximately 5% of SGP retrievals and 22% of AIRS II retrievals indicate scattering. MWR values for each point plotted in Figures 4 and 5 indicate the mean LWP for a 2-hour period around the corresponding AMSR-E observation time; horizontal error bars indicate the corresponding standard deviation. Statistical results presented in Table 3 include coefficient of determination (r^2), least squares fit parameters (with associated uncertainties) and AMSR-E clear-sky error statistics (for which corresponding MWR retrievals of LWP were less than 0.05 mm). Figures 4 and 5 also include AMSR-E LWP retrieval statistics (mean and standard deviation) for each MWR LWP bin of width 0.1 mm (e.g., −0.05 to 0.05 mm, 0.05 to 0.15 mm, etc.). Binned results are plotted over the overpass data as large black diamonds with vertical error bars.

4.2.2. Satellite Comparisons

[29] For one overpass of the SGP region on 3 December 2003, LWP retrievals based on AMSR-E observations were compared with corresponding retrievals derived from the MODIS (the Moderate Resolution Imaging Spectrometer) instrument [*King et al.*, 2003] on Aqua (the same platform as AMSR-E). Although MODIS-based LWP retrievals have not yet been extensively validated, the use of MODIS observations for evaluating AMSR-E LWP retrievals effectively eliminates problems related to sampling time and area. For each AMSR-E retrieval grid cell, the mean MODIS LWP value was obtained by averaging MODIS LWP retrievals for simultaneous observations geolocated in the same cell. Corresponding maps of LWP retrieved by AMSR-E and MODIS for the Aqua overpass occurring at approximately 1936 UTC on 3 December 2003 are shown in Figure 6. A scatterplot of the same data is presented in Figure 7 and the statistical results are presented in the last row of Table 3. At the time of the overpass, archived NEXRAD imagery do not reveal any precipitation in the region. Similarly, the AMSR-E scattering filter did not identify any scattering in this particular scene either.

5. Data Analysis

[30] Analysis of AMSR-E and MWR LWP comparisons is much simpler in clear-sky conditions than during periods of significant cloudiness. Specifically, in clear-sky scenes, the "true" LWP is known to within a small uncertainty, and LWP spatial variability over the retrieval grid cell should be negligible. Other sources of retrieval error, including scattering from precipitating particles, are also minimized in clear-sky scenes. On the other hand, other important potential sources of retrieval error, including instrumental errors, ancillary data errors and variability of $R(\epsilon)$ are not expected

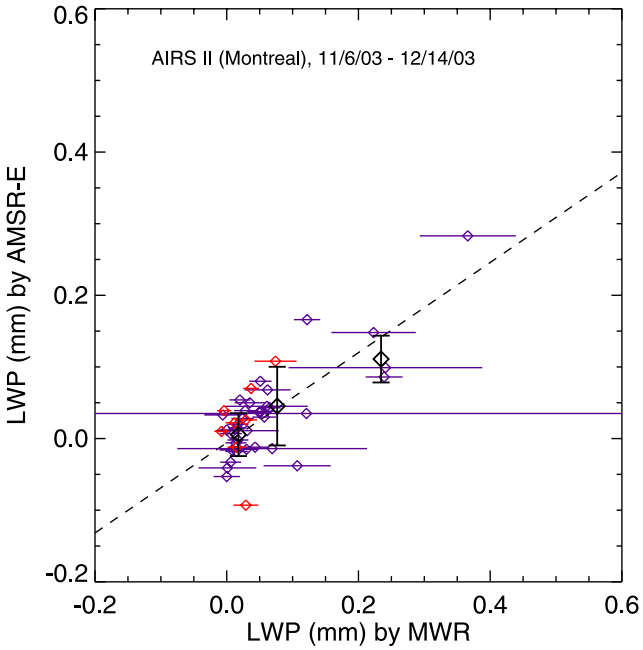

Figure 5. Scatterplot of LWP values retrieved using the AMSR-E dual-frequency method and corresponding MWR values obtained during the AIRS II field campaign. AMSR-E retrievals for which brightness temperatures indicated high scattering are plotted in red. Parameters for least squares fit line (dashed) are listed in Table 3.

Table 3. Comparisons of LWP Retrieval Results by Ground-Based MWR and AMSR-E Described in Section 4.2.1[a]

		Least Squares Fit			Clear-Sky Error Statistics	
Validation Site	PDP Training Set	Offset, mm	Slope	r^2	Bias, mm	RMS Error, mm
SGP	M1	−0.0056 ± 0.0036	0.57 ± 0.03	0.41	−0.0092	0.058
SGP	N1	−0.0040 ± 0.0036	0.51 ± 0.03	0.41	−0.0079	0.057
SGP	N2	−0.0018 ± 0.0038	0.53 ± 0.03	0.40	−0.0057	0.061
SGP	N3	−0.030 ± 0.0038	0.58 ± 0.03	0.38	−0.033	0.062
Mirabel	M1	−0.0059 ± 0.0087	0.63 ± 0.08	0.65	0.0038	0.030
MODIS[b]	M1	0.0019 ± 0.0057	0.63 ± 0.03	0.64	0.012	0.044

[a]Results are in mm.
[b]Results of AMSR-E/MODIS comparisons for the SGP region for an overpass on 3 December 2003 (see section 4.2.2).

to be different during clear and cloudy conditions. Thus analysis of AMSR-E retrieval errors in clear-sky scenes indicates the magnitude of at least an important subset of the entire set of retrieval error sources. For validation purposes, we define all scenes for which the mean MWR LWP over a 2-hour period around the AMSR-E observation time was less than 0.05 mm as clear. We further assume that clear-sky conditions at the MWR location extended throughout the overlapping 0.25° by 0.25° latitude/longitude grid cell. Defined this way, clear-sky scenes constituted about 76% of all SGP scenes and 42% of all AIRS II scenes. As indicated in Table 3, clear-sky bias and RMS error values for all SGP and AIRS II comparisons are typically about 0.01 and 0.06 mm, respectively. These values are consistent with the uncertainty σ_{LWP} calculated in section 3.2.2.

[31] Because of large differences in sampling area, comparisons of AMSR-E and MWR retrieval results in cloudy conditions depend on LWP variability over a large area. To clearly distinguish differences in AMSR-E and MWR retrieval results due to LWP spatial variability from actual retrieval errors would require additional instrumentation (e.g., multiple ground-based radiometers deployed within a single AMSR-E grid cell) to characterize the LWP over an extended region. The lack of such measurements currently prevents true validation of the AMSR-E based method in cloudy conditions [*Wentz and Meissner*, 2000]. Nevertheless, for both the SGP and AIRS II data sets, there exists a clear correlation between AMSR-E and MWR LWP values. Calculated values for the coefficient of determination (r^2) for the SGP and AIRS II data (excluding the observations indicating strong scattering) are approximately 0.4 and 0.6, respectively. The correlation is even more compelling for the binned results. Specifically, the binned results shown in Figure 4 exhibit excellent correlation throughout the entire range of LWP.

[32] AMSR-E retrievals for all of the SGP comparisons were repeated using the M1, N1, N2, and N3 regression coefficients. A comparison of the statistics for these four cases (presented in Table 3) reveals only a marginal dependence on the training set used to produce the PDP regression coefficients. Differences in the clear-sky retrieval bias due to the choice of training set are less than 0.03 mm. Slope values vary between 0.51 and 0.58. These differences generally produce retrieval results which differ by significantly less than the expected retrieval errors (as indicated in Figure 2). These findings suggest that in midlatitude continental conditions, possible regional and seasonal dependences of the PDP regression coefficients do not propagate into large differences in retrieved LWP.

[33] Correlation statistics tabulated in Table 3 are based on MWR values averaged within 2-hour windows as described above. Correlation statistics were also calculated after doubling the MWR window to span a 4-hour period around the AMSR-E observation time. However, results of this experiment were not appreciably different than the results obtained using the standard 2-hour window. Specifically, the coefficient of determination (r^2) increased slightly (from 0.41 to 0.44), the least squares offset decreased slightly (from −0.0056 to −0.0076 mm) and the least squares slope increased slightly (from 0.57 to 0.59). Thus we find that the mismatch in sampling areas of the two measurements can strongly affect LWP disparities for individual overpasses, but have little effect on the correlation statistics for the entire validation data set.

[34] Comparisons of AMSR-E LWP retrieval results with MWR-based and MODIS-based results at multiple sites are well correlated (especially after binning), but also indicate a persistent negative bias of approximately 40–50%. Conceivable sources for this apparent bias include (1) errors in the forward radiative transfer model underlying the PDP, (2) parameterization errors associated with the PDP, (3) possible nonlinearity in the retrieval algorithm (coupled with LWP spatial variability) and (4) systematic errors in the MWR and MODIS retrieval algorithms. Both the error analysis presented in section 3.2.2 and the retrieval simulations presented in section 3.2.3 suggest that parameterization error is an unlikely source for the bias. The observation (made in the previous paragraph) that the width of the MWR averaging window has little effect on the bias suggests that LWP spatial variability is probably not linked with the bias either. We believe errors in the model for the dielectric constant of liquid water used in the forward model calculations [*Liebe et al.*, 1991] are the most likely source for the bias. Our validation results suggest that this model may overestimate the absorption coefficient at 89 GHz.

6. Conclusion

[35] All satellite-based methods for retrieving LWP suffer from fundamental limitations. No method based on any single instrument will likely ever be capable of retrieving LWP in all conceivable situations (with respect to solar illumination, surface type, and cloud structure) with high accuracy. Therefore, to support widely varying applications, new methods which complement the capabilities of current established techniques are highly desired. We have developed and demonstrated a new ''stand-alone'' satellite-based method for retrieving LWP in nonprecipitating clouds over land using passive microwave observations from the

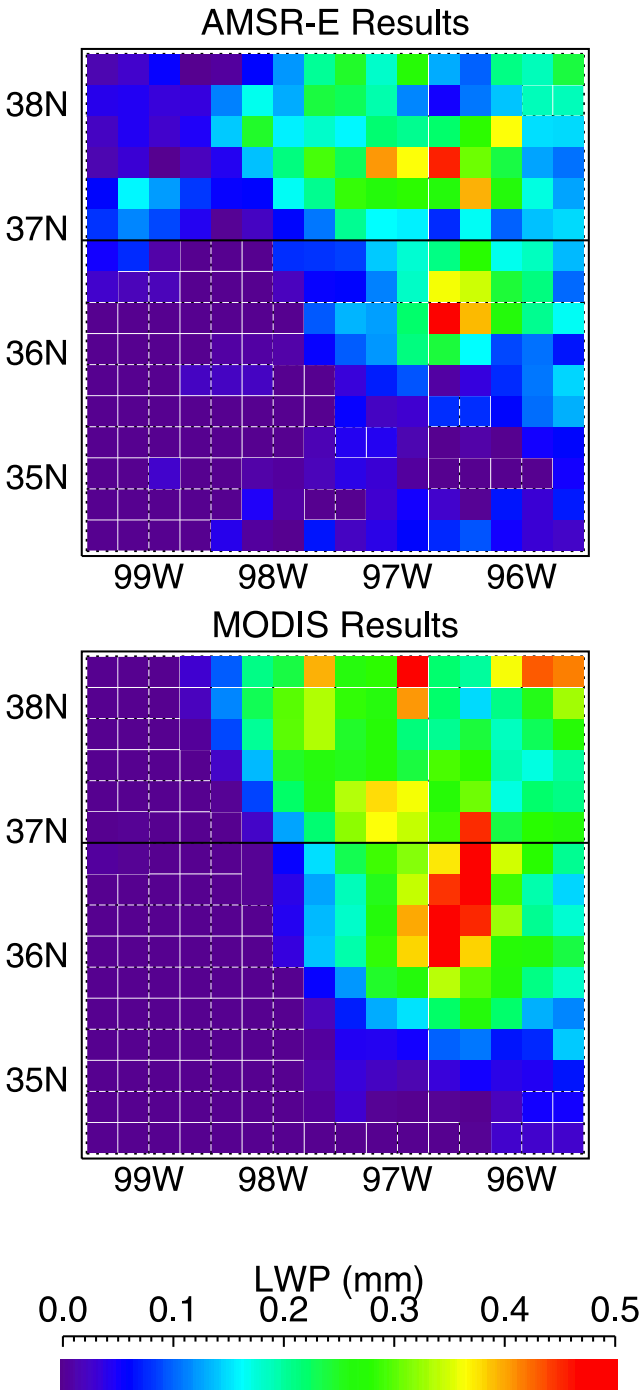

Figure 6. Comparison of AMSR-E and MODIS LWP retrieval results (commonly gridded) for overpass of SGP region at 1936 UTC on 3 December 2003.

AMSR-E instrument. Unlike existing methods based on visible/infrared radiances, the new method is applicable day and night and is insensitive to the presence of overlying cirrus clouds. Unlike the previous NPD method, the new method does not rely on independent clear-sky observations for each scene, nor does it require ancillary satellite measurements to distinguish clear and cloudy conditions.

[36] The new method is built around a new parameterization which simply relates AMSR-E polarization-difference signals to two surface parameters (temperature and $\Delta\epsilon$) and two atmospheric parameters (LWP and PWV). Fundamentally different methods for calculating the parameterization coefficients ultimately produce only weak variability in the LWP retrieval results. Thus the parameterization seems valid over highly variable atmospheric conditions.

[37] For the Southern Great Plains region in the United States, theoretical estimates and MWR-based validation results both indicate LWP root-mean-square errors close to 0.06 mm in clear-sky conditions. Results for cloudy conditions are subject to large random errors because of the large disparity between the sampling areas of the MWR instrument and the AMSR-E retrieval grid cell. Such errors are greatly reduced using a binning technique. Application of binning to both AMSR-E/MWR comparisons and AMSR-E/MODIS comparisons reveals strong underlying correlations over the entire range of LWP. However, these results also strongly indicate a tendency of the AMSR-E results to underestimate the LWP by 40 to 50%. Further investigations will examine possible sources and corrective schemes for this bias.

[38] Further validation will be required to demonstrate the applicability of the new method over surface types distinctly different from those found in the SGP and Montreal regions. The sparseness of operational ground-based MWR instruments (like those deployed at the ARM SGP site) favors other satellite-based methods (e.g., MODIS) for validating AMSR-E retrievals in other regions. Retrieval errors are expected to increase as surface emissivity values approach unity (where $\Delta\epsilon$ tends toward zero); densely forested regions will probably be the most challenging case. However, the similarity of $\Delta\epsilon$ values at 37 and 89 GHz, which the dual-frequency method described here assumes, appears

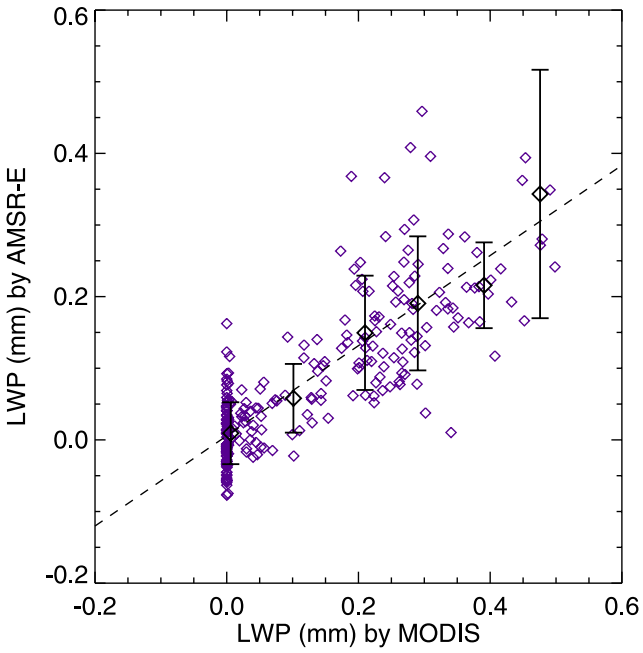

Figure 7. Scatterplot of AMSR-E and MODIS LWP retrieval results shown in Figure 6.

valid over a wide variety of land surface types in North America [*Ruston and Vonder Haar*, 2004]).

Appendix A: Isothermal Model for Polarization-Difference Signal

[39] A simplification to equation (1) occurs in the case of an isothermal atmosphere, with the surface temperature T_S and atmospheric temperature T_A identical. This simplified model is useful for identifying the dominant atmospheric component to equation (1).

[40] If radiative scattering processes in the atmosphere are neglected, the observed TOA microwave brightness temperature is equal to the sum of contributions from (1) upwelling atmospheric emission, (2) surface emission attenuated by the intervening atmosphere, and (3) downwelling atmospheric emission reflected (i.e., scattered) by the surface and attenuated by the atmosphere. At nonnadir viewing angles, the surface emissivity ϵ (which modulates the two latter terms) is generally different for radiation polarized parallel to the plane of incidence (V) and perpendicular to the plane of incidence (H). In contrast, atmospheric emission is typically unpolarized. For an isothermal atmosphere, the sum of the radiance contributions can be simply written

$$T_B^i = \epsilon_A T_A + \epsilon_s^i T_S \mathcal{T} + \epsilon_A T_A \left(1 - \epsilon_s^i\right)\mathcal{T} \tag{A1}$$

where ϵ_A is the atmospheric emissivity, $\mathcal{T}$ is the atmospheric transmittance (from the surface to TOA) and i is a superscript denoting the radiation polarization state. The polarization-difference signal then becomes

$$\Delta T_B = T_B^V - T_B^H = \left(\epsilon_s^V - \epsilon_s^H\right)(T_S - \epsilon_A T_A)\mathcal{T} \tag{A2}$$

(This equation could also be derived from equation (1), since $T_D = \epsilon_A T_A$ in the case of an isothermal atmosphere.) If we also assume that $T_S = T_A$, the polarization signal becomes simply

$$\Delta T_B = \Delta\epsilon T_S \mathcal{T}^2 \tag{A3}$$

since $\mathcal{T} = (1 - \epsilon_A)$ by Kirchoff's Law. Thus, for the isothermal case, the dependence of ΔT_B on the atmospheric absorbers including water vapor and cloud liquid is contained solely in the term $\mathcal{T}^2$. Assuming height-independent extinction coefficients for fixed gases, water vapor, and cloud liquid, equation (A2) becomes

$$\Delta T_B = \Delta\epsilon T_S \exp\left[-2(\tau_0 - \alpha_1 LWP - \alpha_2 PWV)\right] \tag{A4}$$

where τ_0 is the optical depth for fixed gases, and α_1 and α_2 are the extinction coefficients for cloud liquid and water vapor. The form of this equation indicates that the dependences of ΔT_B on LWP and PWV are dominated by an exponential term.

[41] **Acknowledgments.** The authors would like to thank the two reviewers for providing valuable suggestions. MWR and MWRP data were obtained from the Atmospheric Radiation Measurement (ARM) Program sponsored by the U.S. Department of Energy, Office of Science, Office of Biological and Environmental Research, Environmental Sciences Division. NCEP Reanalysis data were provided by the NOAA-CIRES Climate Diagnostics Center, Boulder, Colorado, USA, from their web site at http://www.cdc.noaa.gov/. AMSR-E data were obtained from the National Snow and Ice Data Center through the EOS Data Gateway at http://redhook.gsfc.nasa.gov/imswww/pub/imswelcome/.

References

Aires, F., C. Prigent, W. B. Rossow, and M. Rothstein (2001), A new neural network approach including first guess for retrieval of atmospheric water vapor, cloud liquid water path, surface temperature, and emissivities over land from satellite microwave observations, *J. Geophys. Res.*, *106*, 14,887–14,907.

Combs, C. L., T. J. Greenwald, A. S. Jones, D. L. Randel, and T. H. Vonder Haar (1998), Satellite detection of cloud liquid water over land using polarization differences at 85.5 GHz, *Geophys. Res. Lett.*, *25*, 75–78.

Deeter, M. N., and J. Vivekanandan (2005), AMSU-B observations of mixed-phase clouds over land, *J. Appl. Meteorol.*, *44*, 72–85.

Dong, X., P. Minnis, G. G. Mace, W. L. Smith Jr., M. Poellot, R. T. Marchand, and A. D. Rapp (2002), Comparison of stratus cloud properties deduced from surface, GOES, and aircraft data during the March 2000 ARM cloud IOP, *J. Atmos. Sci.*, *59*, 3265–3284.

Ferraro, R. R., N. C. Grody, and G. F. Marks (1994), Effects of surface conditions on rain identification using the SSM/I, *Remote Sens. Rev*, *11*, 195–209.

Greenwald, T. J., C. L. Combs, A. S. Jones, D. L. Randel, and T. H. Vonder Haar (1997), Further developments in estimating cloud liquid water over land using microwave and infrared satellite measurements, *J. Appl. Meteorol.*, *36*, 389–405.

Greenwald, T. J., C. L. Combs, A. S. Jones, D. L. Randel, and T. H. Vonder Haar (1999a), Error estimates of spaceborne passive microwave retrievals of cloud liquid water over land, *IEEE Trans. Geosci. Remote Sens.*, *37*, 796–804.

Greenwald, T. J., S. A. Christopher, J. Chou, and J. C. Liljegren (1999b), Intercomparison of cloud liquid water path derived from the GOES 9 imager and ground-based microwave radiometers for continental stratocumulus, *J. Geophys. Res.*, *104*, 9251–9260.

Gueldner, J., and D. Spaenkuch (2001), Remote sensing of the thermodynamic state of the atmospheric boundary layer by ground-based microwave radiometry, *J. Atmos. Oceanic Technol.*, *18*, 925–933.

Hollinger, J. P., J. L. Pierce, and G. A. Poe (1990), SSM/I instrument evaluation, *IEEE Trans. Geosci. Remote Sens.*, *28*, 781–791.

King, M. D., W. P. Menzel, Y. J. Kaufman, D. Tanre, B. C. Gao, S. Platnick, S. A. Ackerman, L. A. Remer, R. Pincus, and P. A. Hubanks (2003), Cloud and aerosol properties, precipitable water, and profiles of temperature and humidity from MODIS, *IEEE Trans. Geosci. Remote Sens.*, *41*, 442–458.

Liebe, H. J., G. A. Hufford, and T. Manabe (1991), A model for the complex permittivity of water at frequencies below 1 THz, *Int. J. Infrared Millimeter Waves*, *12*, 659–675.

Liljegren, J. C., E. E. Clothiaux, G. G. Mace, S. Kato, and X. Dong (2001a), A new retrieval for cloud liquid water path using a ground-based microwave radiometer and measurements of cloud temperature, *J. Geophys. Res.*, *106*, 14,485–14,500.

Liljegren, J. C., B. M. Lesht, S. Kato, and E. E. Clothiaux (2001b), Evaluation of profiles of temperature, water vapor, and cloud liquid water from a new microwave radiometer, paper presented at Eleventh ARM Science Team Meeting, U.S. Dep. of Energy, Atlanta, Ga.

Lin, B., and P. Minnis (2000), Temporal variations of land surface microwave emissivities over the Atmospheric Radiation Measurement program Southern Great Plains site, *J. Appl. Meteorol.*, *39*, 1103–1116.

McClatchey, R. A., R. W. Fenn, J. E. A. Selby, F. E. Volz, and J. S. Garin (1972), Optical properties of the atmosphere, 3rd ed., *Rep. AFCRL-047297*, Air Force Cambridge Res. Lab., Bedford, Mass.

Muller, B. M., H. E. Fuelberg, and X. Xiang (1994), Simulations of the effects of water vapor, cloud liquid water, and ice on AMSU moisture channel brightness temperatures, *J. Appl. Meteorol.*, *33*, 1133–1154.

Njoku, E. G., T. J. Jackson, V. Lakshmi, T. K. Chan, and S. V. Nghiem (2003), Soil moisture retrieval from AMSR-E, *IEEE Trans. Geosci. Remote Sens.*, *41*, 215–229.

Ohring, G., S. Lord, J. Derber, K. Mitchell, and M. Ji (2002), Applications of satellite remote sensing in numerical weather and climate prediction, *Adv. Space Res.*, *30*, 2433–2439.

Prigent, C., W. B. Rossow, and E. Matthews (1997), Microwave land surface emissivities estimated from SSM/I observations, *J. Geophys. Res.*, *102*, 21,867–21,890.

Riley, R. K. (1998), Mixed-phase icing conditions: A review, *Rep. DOT/FAA/AR-98/76*, 45 pp., U.S. Dep. of Transp., Washington, D. C.

Ruston, B. C., and T. H. Vonder Haar (2004), Characterization of summertime microwave emissivities from the Special Sensor Microwave Imager

over the conterminous United States, *J. Geophys. Res.*, *109*, D19103, doi:10.1029/2004JD004890.

Slingo, A. (1989), GCM parameterization for the short-wave radiative properties of water clouds, *J. Atmos. Sci.*, *46*, 1419–1427.

Weng, F., and N. C. Grody (1994), Retrieval of cloud liquid water using the special sensor microwave imager (SSM/I), *J. Geophys. Res.*, *99*, 25,535–25,551.

Wentz, F. J., and T. Meissner (2000), AMSR Ocean Algorithm: Algorithm Theoretical Basis Document, version 2, *RSS Tech. Proposal RSS121599A-1*, Remote Sens. Syst., Santa Rosa, Calif. (Available at http://eospso.gsfc.nasa.gov/eos_homepage/for_scientists/atbd).

Zuidema, P., E. R. Westwater, C. Fairall, and D. Hazen (2005), Ship-based liquid water path estimates in marine stratocumulus, *J. Geophys. Res.*, *110*, D20206, doi:10.1029/2005JD005833.

M. N. Deeter and J. Vivekanandan, National Center for Atmospheric Research, P.O. Box 3000, Boulder, CO 80307, USA. (mnd@ucar.edu)